RSC Advances

PAPER

View Article Online
View Journal | View Issue

Check for updates

Cite this: *RSC Adv.*, 2026, **16**, 26488

Phosphoric acid-activated biochars from orange and potato peels as adsorption barriers to prevent picloram and imidacloprid leaching in contaminated soils

Jorge Vidal, *[a] María E. Báez,[b] Francisco Garrido Morales,[a] Andrés Yar[a] and Abdoulaye Thiam[c]

This study investigated the potential of H_3PO_4-activated biochar from agricultural waste as an adsorption barrier to mitigate groundwater contamination by picloram and imidacloprid. The biochars exhibited high surface areas, mesoporous structures, and high porosity. The maximum adsorption capacity and influence of experimental variables (adsorbent mass, initial concentration, pH, contact time, and temperature), along with their interactions, were assessed using response surface methodology. Predicted maximum capacities were 51 μg mg^{-1} for picloram and 66 μg mg^{-1} for imidacloprid. The most significant effects were the adsorbent mass and initial concentration, whereas temperature was non-significant. Although pH significantly affected the adsorption of picloram, adsorption remained high under environmentally relevant pH conditions. Kinetic and equilibrium data were best described by the pseudo-second order and Freundlich models, respectively, indicating rapid uptake and heterogeneous multilayer adsorption. Furthermore, 96% of imidacloprid and 65% of picloram remained adsorbed after three desorption cycles. Matrix effects, evaluated in soils with negligible adsorption capacity, were more pronounced for picloram. Nevertheless, amending with a low dose of biochar (0.5% w/w) increased K_d values by 8 (picloram) and 120-fold (imidacloprid). In soil column experiments (100 g), the addition of a low-dose biochar barrier (20 mg for imidacloprid and 100 mg for picloram, mixed with 1 g of soil) effectively limited leaching to 12–24% and 25–30%, respectively, depending on the soil type. Overall, these results demonstrate that biochar derived from agricultural waste is an effective and sustainable amendment for pesticides immobilization, providing a promising strategy for mitigating soil and groundwater pollution.

Received 3rd November 2025
Accepted 2nd May 2026

DOI: 10.1039/d5ra08466k

rsc.li/rsc-advances

Open Access Article. Published on 18 May 2026. Downloaded on 5/20/2026 7:35:47 PM.
This article is licensed under a Creative Commons Attribution-NonCommercial 3.0 Unported Licence.

1. Introduction

According to the United Nations' World Population Prospects 2024, the global population grew from 2.5 billion in 1950 to 7.8 billion in 2020 and is projected to reach 9.7 billion by 2050.[1] Consequently, the growing demand for food has led to a progressive increase in the use and production of pesticides over recent decades to ensure sufficient agricultural output. Only a small fraction of applied pesticides reach their final biological target, while a significant portion remains in the environment, accumulating in soils and sediments. Others can reach wells, rivers, and lakes or leach through the soil, contaminating groundwater and becoming potentially toxic to non-target organisms.[2–4] The acidic herbicide Picloram (PCM, 4-amino-3,5,6-trichloropyridine-2-carboxylic acid) has a low pK_a value and is weakly adsorbed on most agricultural soils, due to electrostatic repulsion between its anionic specie and the negatively charged organo-mineral components of the soil. Furthermore, its water solubility and relatively high persistence contribute to its high mobility in soils, increasing the risk of contamination of surface and groundwater.[5–9] On the other hand, the neonicotinoid insecticide imidacloprid (IMI, 1-(6-chloro-3-pyridylmethyl)-*N*-nitroimidazolidin-2-ylideneamine) also has a high-water solubility; it is non-dissociable and can be adsorbed on soil components only through weak forces such as H-bonding and van der Waals interactions.[10–12] Furthermore, its high persistence in soils increases the possibility to migrate into groundwater. The detection of these contaminants in surface and groundwater related to areas of intensive agricultural activity has been frequently reported in the literature.[3,4,9,13–17] Both compounds pose a significant risk to a diverse range of

[a]*Grupo de Investigación en Remediación Medio Ambiental (GIREMA), Departamento de Química de los Materiales, Facultad de Química y Biología, Universidad de Santiago de Chile, Chile. E-mail: jorge.vidal.f@usach.cl*

[b]*Departamento de Química Inorgánica y Analítica, Facultad de Ciencias Químicas y Farmacéuticas, Universidad de Chile, Chile*

[c]*Instituto Universitario de Investigación y Desarrollo Tecnológico, Universidad Tecnológica Metropolitana, Santiago, Chile*

© 2026 The Author(s). Published by the Royal Society of Chemistry

Open Access Article. Published on 18 May 2026. Downloaded on 5/20/2026 7:35:47 PM. This article is licensed under a Creative Commons Attribution-NonCommercial 3.0 Unported Licence.

aquatic and terrestrial organisms. Recent studies have reported behavioral changes of farmland birds, a decline in aquatic insect populations, and sublethal adverse effects on fish early life stages because of exposure to IMI.[18–20] On the other hand, this compound has been identified as posing a high ecological risk because the concentrations determined in soils in agricultural areas can produce sublethal, acute, or detrimental effects on non-target invertebrate species.[21–23] The effect on survival, egg productivity, and length of nematodes and the genotoxic effects on amphibians has also been reported for PCM.[24,25] Additionally, IMI and PCM can induce changes in the structure, abundance, genetic diversity, and metabolic activity of soil microbial communities.[26,27] Considering the potential long-term threat to the quality and biodiversity of terrestrial and aquatic environments, together with the increasing global demand for clean water supplies and uncontaminated products for human consumption, the above discussion highlights the need for effective soil immobilization of PCM and IMI in contaminated soils as a viable strategy for remediation.

Adsorption represents a cost-effective alternative for the remediation of soil contaminated with organic compounds, and biochar is among the most widely used adsorbents for this purpose. Owing to its high specific surface area and porous structure, biochar exhibits a strong sorption capacity for pesticides in soil environments. However, its effectiveness in pesticide sorption–desorption process depends on characteristics determined by the feedstock and pyrolysis conditions used. These conditions influence properties such as porosity, surface charge, functional groups, carbon content, aromaticity, and mineralogical composition.[28] In recent years, the adsorption capacity produced from various sources has been substantially improved using different activation methods. Thus, phosphoric acid-activated biochar has been successfully applied as adsorbent of a wide type of organic contaminants in aquatic environment.[29] The better performance is attributed to the better surface properties. The possibility to form phosphate bond with organic matter in biomass helps the micropores formation. Additionally, the modification increases the specific surface area, the total pore volume, and adsorption sites, and favors the presence of diverse surface functional groups.[29,30] Adsorption mechanisms such as oxygen-containing functional group complexation, π–π interactions, ion exchange, H-bonding, van der Waals forces, electrostatic interactions, and hydrophobic interactions have been reported.[30–33] Due to the stability of their structures and the multiple possible interaction mechanisms, these materials have achieved great efficiency in removing contaminants such as antibiotics,[34–37] pesticides,[30,38] and dyes,[31,39,40] widely distributed in water and soil.

Currently, research has focused on the synthesis of eco-friendly adsorbents using inexpensive raw materials such as agricultural and domestic waste. Among these, fruit and vegetable residues can be used as low-cost raw materials to obtain products with enhanced adsorption capacity.[41,42] Thus, potato peels were used to produce activated biochar with formic and sulfuric acids with a high adsorption of malachite green in aqueous solution.[43] On the other hand, grapefruit peel activated with phosphoric acid was successfully used to remove methyl orange from wastewater.[40]

Considering the high risk of groundwater contamination with PCM and IMI, this study aimed to assess the possibility of introducing a biochar-based barrier with high adsorption capacity for both compounds into soils. To this purpose, the adsorption–desorption process of PCM and IMI on phosphoric acid-activated biochar derived from potato and orange peels in aqueous media was first investigated. The effects of different soil matrices, which could affect the efficiency of both adsorbents, were then evaluated. Finally, the feasibility of using these adsorbents as a low-dose retention barrier to immobilize both contaminants without altering soil's physical and chemical properties was established in soil columns. Our findings provide a scientific basis for developing sustainable remediation strategies to protect groundwater from pesticide contamination by integrating unconventional feedstocks, with a closer approximation of laboratory studies to their potential application under field conditions.

2. Materials and methods

2.1 Chemical reagents

Picloram (CAS number: 1918-02-1, $C_6H_3Cl_3N_2O_2$, 99.9% purity) and imidacloprid (CAS number: 138261-41-3, $C_9H_{10}ClN_5O_2$, 99.9% purity) were provided by Sigma-Aldrich. The principal properties of these compounds are described in SI, Table S1. Ultrapure water was obtained from a Synergy® water purification system (Merck Millipore), and HPLC-grade acetonitrile was supplied by Merck. Other reagents (HCl, NaOH, H_3PO_4, and $CaCl_2$, analytical grade) were also obtained from Merck.

2.2 Soils

Two volcanic soils representative of the Ultisol order and one non-volcanic soil representative of the Mollisol order were used to assess the soil matrix effect: Metrenco (MET, depth 40–60 cm; 38.8° S, 72.6° W), Collipulli (COLL, depth 15–30 cm, 37.9° S, 72.4° W), and Olivar (OLV, depth 0–20 cm, 34.2° S, 70.8° W), respectively. The corresponding OC content, pH, and CEC were 1.5%, 5.6, and 35.5 meq (+)/100 g (MET), 1.8%, 5.3, and 39.1 meq (+)/100 g (COLL), and 1.9%, 6.9, and 14.7 meq (+)/100 g (OLV).

2.3 Preparation of biochars

Waste orange and potato peels were collected as raw materials and treated identically. The peels were repeatedly washed with distilled water to remove contaminants and then dried at 70 °C for 24 hours. After drying, the peels were ground and sieved to obtain particles smaller than 45 μm. Following this pretreatment, the activation process was conducted as follows. The peel powder was mixed with 85% H_3PO_4 in a ratio of 1 : 2.5 (g peel powder : g acid) and stirred for 10 hours. The mixture was placed in a muffle furnace at 450 °C for 60 minutes. After calcination, the material was washed with distilled water. This step was repeated until the pH of the wash water remained constant, 3 for orange peel biochar (OPB) and 4.5 for potato peel

Open Access Article. Published on 18 May 2026. Downloaded on 5/20/2026 7:35:47 PM. This article is licensed under a Creative Commons Attribution-NonCommercial 3.0 Unported Licence.

biochar (PPB). Finally, the material was dried at 60 °C for 10 hours.

2.4 Characterization of adsorbents

FESEM images of activated biochar samples were obtained before and after the adsorption of PCM and IMI using a Zeiss GeminiSEM 360, while elemental analysis was performed with a coupled Oxford EDS detector, Ultim Max 40. FTIR spectra were obtained in the same samples by using a Spectrum Two spectrometer with the ATR diamond accessory (PerkinElmer) in the range of 4000 cm^{-1} and 400 cm^{-1} with a resolution of 1 cm^{-1}.

N_2 adsorption/desorption isotherms study was performed at −196 °C in a relative pressure range of p/p^0 = 0–1 using a Micromeritics 3Flex system. Samples were previously degassed under vacuum at 300 °C (ramping at 10 °C min^{-1}) with a Micromeritics Smart VacPrep unit. The specific surface areas were determined *via* the Brunauer, Emmett, and Teller (BET) method. The total pore volume was calculated from the adsorbent amount at a p/p^0 ratio of 0.990. The micropore volume and area were determined using the *t*-plot method. The mesopore volume was calculated as the difference between the total pore volume and the micropore volume, while the mesopore area was obtained as the difference between the total specific surface area and that corresponding to the microporous fraction.

The temperature-programmed decomposition (TPD) of biochars was determined with a Micromeritics 3Flex system equipped with a thermal conductivity detector (TCD) and coupled to an MKS Cirrus 2 mass spectrometer. The measurements were conducted under a helium flow (100 mL min^{-1}) with a heating rate of 10 °C min^{-1} up to 1000 °C. The mass-to-charge (*m*/*z*) fragments recorded were 15, 18, 28, and 44, corresponding to CH_4, H_2O, CO, and CO_2, respectively. The CO and CO_2 signals were quantified by calibrating the detector with calcium oxalate as a standard. These TPD analyses provided information about CO, CO_2, and H_2O emissions produced by the decomposition of the samples.

To determine the surface charge of biochar, the zeta potential was measured as a function of pH using a Zetasizer Nano ZS (Malvern Panalytical). Samples were suspended in deionized water (0.125 g L^{-1}), and the pH was adjusted from 3.0 to 12.0 using 0.1 mol per L HCl and 0.1 mol per L NaOH solutions.

2.5 Effects of experimental factors on the adsorption of PCM and IMI on biochars

The individual effects and the interaction between experimental variables, and the optimum conditions for PCM and IMI adsorption on the activated biochars were studied through Response Surface Methodology (RSM) by using a Döehlert design. Based on preliminary studies, conducted to define the domain of factors, OPB and PPB were selected for the study of PCM and IMI, respectively. The experimental factors considered for PCM adsorption were: OPB mass (A; 5 to 15 mg), PCM concentration (B; 5 to 50 μg mL^{-1}), pH (C; 2 to 9), and contact time (D; 12 to 107 min). The number of levels used for each factor was 7, 7, 5, and 3, respectively. All experiments were conducted at 25 °C. For IMI adsorption, the experimental factors were: PPB mass (A; 5 to 15 mg), IMI concentration (B; 5 to 50 μg mL^{-1}), and temperature (C; 10 to 30 °C), and the respective number of levels was 5, 7, and 3. In this case, the final solutions pH was 3.8. The response variable in both cases was the amount of PCM and IMI adsorbed, expressed in μg mg^{-1} of biochar. The experiments were performed in a randomized block design. A total of 30 experiments were conducted for PCM, comprising 21 factorial points, three replicates of the central point, and seven random duplicate points. For IMI, the total number of experiments was 19, including 13 factorial points, three replicates corresponding to the central point, and four random duplicate points. The coded and real variable values in the Döehlert experimental matrix are shown in Tables S2 and S3. Concentrated standard solutions of PCM and IMI (1000 μg mL^{-1}) were prepared in acetonitrile and then diluted with ultrapure water modified at the pH and initial concentration required for each experiment. 10 mL of these solutions were added to glass tubes with the corresponding amount of biochar. The final concentration of ACN for each solution was 2% v/v. The assays were carried out at controlled temperature (25 °C) and constant agitation in a vertical tube rotator, according to the times established in the experimental designs. Then, the samples were centrifuged at 15 000 rpm for 20 min at 4 °C and analyzed by HPLC-DAD. The agitation and centrifugation steps, and the analytical determination of pesticides were applied in the same way in all subsequent studies.

2.5.1 Kinetic and isotherm studies. To study the adsorption kinetics of PCM and IMI on OPB and PPB, respectively, two different batch experiments were performed. In the first experiment, the pesticide concentration was kept constant (25 μg mL^{-1}) while the adsorbent mass was varied by using 5 and 10 mg of OPB and PPB. In the second experiment, the biochar amount was kept constant (7.5 mg) while the concentration of PCM and IMI was varied by using 15 and 35 μg mL^{-1} (all in duplicates). The pH and temperature conditions were 5.5 and 25 °C, and the equilibration times were 2, 4, 6, 8, 10, 12, 15, 20, 25, and 30 minutes.

The data derived from the kinetic adsorption experiments were fitted to the pseudo-first-order (eqn (1)), pseudo-second-order (eqn (2)), and intraparticle diffusion models (eqn (3))

$$q_t = q_{max}[1 - e^{-k_1 t}] \quad (1)$$

$$q_t = \frac{k_2 {q_{max}}^2 t}{1 + k_2 q_{max} t} \quad (2)$$

$$q_t = k\sqrt{t} \quad (3)$$

where, q_t is the adsorbed amount of the adsorbate at time t, q_{max} is the maximum adsorption capacity, and k_1, k_2, and k are the pseudo-first and second order and intraparticle diffusion rate constants, respectively.

Adsorption isotherm experiments were conducted by using 10 mL of PCM and IMI solutions prepared at different concentrations (5, 10, 15, 20, 25, 30, 35, 40, 45, and 50 μg mL^{-1}) and 7.5 mg of the selected adsorbent (all in duplicates). The initial solution pH was adjusted to 5.5, and the equilibration time was 30 min. According to the results obtained through the

© 2026 The Author(s). Published by the Royal Society of Chemistry

Open Access Article. Published on 18 May 2026. Downloaded on 5/20/2026 7:35:47 PM. This article is licensed under a Creative Commons Attribution-NonCommercial 3.0 Unported Licence.

RSM, the temperature effect on the adsorption capacity of adsorbents was established only for PCM on OPB samples. The temperatures used were 15, 25, and 35 °C, while for IMI on PPB the temperature was set at 25 °C. Data were fitted to the Langmuir (eqn (4)), Freundlich (eqn (5)), and Dubinin–Radushkevich (eqn (6)–(8)) models.

$$q_e = \frac{q_{max} K_L C_e}{1 + K_L C_e} \quad (4)$$

$$q_e = K_F C_e^{1/n} \quad (5)$$

$$q_e = q_{max}\, e^{-K_{DR}\varepsilon^2} \quad (6)$$

$$\varepsilon = RT \ln \frac{c_s}{c_e} \quad (7)$$

$$E = \frac{1}{\sqrt{2K_{DR}}} \quad (8)$$

where for the Langmuir and Freundlich models, q_e is the adsorbed amount of the adsorbate, c_e is the equilibrium concentration in solution, q_{max} is the maximum adsorption capacity, K_L is the Langmuir constant, K_F is the Freundlich constant, and n is the dimensionless intensity parameter. For the Dubinin–Radushkevich model K_{DR} is the constant, q_{max} is the maximum adsorption capacity, ε is the adsorption potential based on the Polanyi's potential theory, c_s and c_e are the saturation concentration or solubility of the adsorbate and the equilibrium concentration in solution, and E is the mean free energy.

For the Dubinin–Radushkevich model, considering that the concentration range investigated was narrow and exhibited a tendency toward saturation in all cases near 50 mg L^{-1}, a higher c_s value (70 mg L^{-1}) was selected for parameter estimation.

The thermodynamic parameters ΔG (kJ mol^{-1}), ΔH (kJ mol^{-1}), and ΔS (J mol^{-1} K^{-1}) were calculated from equilibrium data obtained for PCM using eqn (9) and (10).

$$\Delta G = -RT \ln K \quad (9)$$

$$\ln K = -\frac{\Delta H}{R}\frac{1}{T} + \frac{\Delta S}{R} \quad (10)$$

where K is the Langmuir constant, T is the temperature in Kelvin, and R is the universal gas constant = 8.314 J mol^{-1} K^{-1}.

2.5.2 Desorption of PCM and IMI from biochar into an aqueous solution. PCM and IMI were initially adsorbed onto biochar using concentrations of 10 and 20 μg mL^{-1}, 7.5 mg of the respective adsorbents, and an equilibration time of 30 min (at 25 °C, all in duplicates). After separating the sediments by centrifugation, they underwent three desorption cycles, each involving 60 min of agitation and the replacement of 9 mL of supernatant with 9 mL of ultrapure water. The concentration of each compound in solution was measured at each step.

2.6 Effects of soil matrix on PCM and IMI adsorption capacity of biochars

To assess the overall adsorption performance of biochar under the influence of real soil matrices, two grams of each soil type were mixed with different amounts of OPB and PPB (5, 7.5, and 10 mg). Adsorption tests were conducted in 50 mL polypropylene centrifuge tubes at 25 °C using an aqueous solution with a concentration of 25 μg mL^{-1}. The samples were equilibrated for 60 min at a pH adjusted to 5.5 (all in duplicates). For comparison, the adsorption capacities of unamended soils and the same amounts of biochar alone were evaluated in the same experimental conditions.

2.7 Vertical transport of PCM and IMI in unamended and amended soil columns

Soils under study (MET, COLL, and OLV) were uniformly packed in poly (methyl methacrylate) columns (22 cm in length and 2.5 cm in internal diameter) occupying 19 cm of the column height (Fig. S1). To prevent soil displacement, a 1 cm layer of glass wool and a 1 cm layer of fine quartz were placed at the bottom of each column. Subsequently, the MET and COLL soils were equilibrated by capillarity with ultrapure water, and the OLV soil with a 0.01 M $CaCl_2$ solution for 24 hours (in this case, to maintain a stable flow rate during the elution). The excess water was drained freely over 10–14 h. The difference in weight before and after the saturation corresponded to the pore volume (PV). The hydrodynamic behavior of soil columns was assessed using tritiated water as a tracer. The experiments were conducted both in the absence and presence of the respective biochar (OPB for PCM and PPB for IMI). 100 g of soil was added to all columns. However, in the columns with amended soil, a barrier consisting of a mixture of 1 g of soil and 100 mg of OPB, or 20 mg of PPB, was placed approximately 4 cm from the top of the soil column, and the column was then filled with the remaining soil (4 g). Aqueous solution (5 mL; at 40 μg mL^{-1} concentration, total 200 μg) of each pesticide was applied to the top of the column at a flow rate of 0.28 mL min^{-1}, controlled through a peristaltic pump (Lambda Preciflow). The same flow rate was used for the elution of compounds with ultrapure water. Fractions of leachates were regularly collected using an Advantec SF-2120 super fraction collector and then analyzed by HPLC-DAD (Fig. S1).

2.8 Analytical determination of PCM and IMI

For the analysis of PCM and IMI in supernatants and eluates, an HPLC system consisting of a quaternary gradient pump (model 600), an autosampler (model 717 Plus), and a DAD detector (model 997), all from waters, was used. The column was a Zorbax Eclipse XDB C18 (5 μm particle size, 150 mm × 4.6 mm i.d.). Wavelengths for the quantification of PCM and IMI were 224 and 270 nm, respectively. Both compounds were determined in isocratic conditions. For PCM, a mobile phase of 20% acetonitrile and 80% ultrapure water acidified to pH 3 and a flow rate of 1.3 mL min^{-1} were used. For IMI, the mobile phase and the flow rate were 40% acetonitrile and 60% ultrapure water, and 1 mL min^{-1}, respectively. The retention times under these conditions were 2.5 and 2.2 min, respectively. Figures of merit of this analytical method are presented in Table S4.

Open Access Article. Published on 18 May 2026. Downloaded on 5/20/2026 7:35:47 PM. This article is licensed under a Creative Commons Attribution-NonCommercial 3.0 Unported Licence.

2.9 Statistical analysis

The statistical significance of each factor and their interactions on the adsorption capacity of each adsorbent (obtained by RSM) was determined by analysis of variance (ANOVA). The significant level was set at p-value < 0.05, and the response used was μg adsorbed per mg of adsorbent (Statgraphics Centurion XV software). Isotherm and kinetic adsorption data were fitted to models through nonlinear regression method (OriginPro 9.0 software).

3. Results and discussion

3.1 Characterization of biochars

SEM images of the surface of OPB and PPB before and after the adsorption of PCM and IMI, respectively, and the corresponding elemental compositions determined by EDS are observed in Fig. 1. This figure reveals a heterogeneous morphology characterized by the presence of pores and grooves of various sizes (A–D). These structural characteristics are consistent with previous studies.[44] Related to the elemental composition in both materials, no differences were found before the adsorption process (E and G), with carbon being the most abundant (79.7%), followed by oxygen (13.5%), and finally phosphorus, originating from the H_3PO_4 used in the activation process (6.8%). However, elemental composition differences were observed after the adsorption process due to the presence of chlorine and nitrogen. In the case of OPB (F), the Cl percentage was 0.7%, while in PPB (H) was 0.2%. This could be attributed to the higher number of chlorine atoms present in the PCM molecule compared to IMI (Table S1). In addition, nitrogen was only detected in PPB (H) because of the higher number of nitrogenous functional groups in the IMI molecule, with a 0.5% content.

The BET method was applied to determine the specific surface area, pore volume, and pore size of the adsorbent materials (Table 1). The nitrogen adsorption/desorption isotherms at 77 K for OPB and PPB are presented in Fig. S2. In both materials, a clear hysteresis loop was observed following a type IV isotherm, characteristic of predominantly mesoporous materials, according to IUPAC classification.[45] As shown in Table 1, OPB exhibited a higher specific surface area than PPB. However, PPB had a slightly higher total pore volume compared to OPB. In contrast, OPB exhibited a more developed microporous structure, as evidenced by its larger microporous surface area (353.5 $m^2\ g^{-1}$) and greater microporous volume (0.15 $cm^3\ g^{-1}$) compared to PPB. This microporosity suggests the presence of adsorption sites within the porous spaces, which could favor adsorption processes governed by pore-filling mechanisms.

The FTIR spectra presented in Fig. 2A and B showed similar profiles for both materials before and after the adsorption process, with the same transmittance bands. A broadband is observed between 3000 and 3600 cm^{-1}, attributed to O–H stretching, associated with hydroxyl groups present in alcohols and phenols of compounds such as cellulose, pectin, and lignin[46] and C–O–P stretching.[33] Likewise, a moderate band is detected at 1698 cm^{-1}, corresponding to C=O stretching, attributable to esters present in lignin and pectin.[47] Another band, located at 1569 cm^{-1} for PPB and 1572 cm^{-1} for OPB, may be associated with C=C stretching in aromatic rings. Additionally, bands at 1120 and 1052 cm^{-1} could correspond to C–O stretching of aliphatic ethers and secondary and primary alcohols present in cellulose, lignin, and pectin. The band at 1170 is characteristic of phosphorus or phosphocarbonaceous compounds corresponding to the stretching vibration of P–O (hydrogen-bonded) groups from phosphates, and to the O–C stretching vibration of P–O–C linkage. A characteristic band around 1075 cm^{-1} is attributed to the ionized linkage P^+–O^- of phosphate and symmetrical stretching vibration from polyphosphate groups[40,48,49] originated from the dehydration reaction by H_3PO_4.

According to the TPD analysis results shown in Fig. 3, a great release of CO between 600 and 900 °C occurs in PPB, whereas in the OPB sample, the release remains constant between 600 and 750° before decreasing significantly. The release of CO at around 700 °C is mainly attributed to the rupture of ether bonds, while in the range of 700 to 900 °C, the evolution of this gas is associated with the decomposition of carbonyl and phenolic groups present in the structure of the material.[50] The PPB and OPB samples exhibit the same functional groups; therefore, PPB would have a higher concentration of these groups. On the other hand, Fig. 3B shows a significant release of H_2O between 100 and 800 °C and no CO_2 release for both biochar samples. Due to the absence of CO_2 release between 50 and 200 °C, the presence of carboxylic groups in both samples was ruled out. This can be attributed to the biochar activation process, where a dehydration reaction occurs between phosphoric acid and the O–H groups in the samples, particularly those from carboxyl groups.

The zeta potential values (mV) shown in Fig. S3 indicate that the OPB and PPB exhibit a negative surface charge across the entire pH range studied (3 to 12). The zeta potentials of OPB and PPB ranged from −8.41 to −29.8 mV and −14.2 to −34.6 mV, respectively. These results are consistent with those reported in the literature,[44] for activated carbon prepared from orange peels in a similar pH range (2 to 11). The observed changes in zeta potential can be attributed to the abundant presence of –OH functional groups, introduced during activation with H_3PO_4, as well as phenolic groups. The evolution of CO observed for PPB in the TPD results indicated a higher number of phenolic groups, which could contribute to its more negative zeta potential values.

3.2 Influence of experimental variables on the adsorption of PCM and IMI on the OPB and PPB

A preliminary study was carried out to evaluate the adsorption capacity of the activated OPB and PPB for both pesticides. The analysis was developed considering two variables: adsorbent mass (5, 10, and 15 mg) and adsorbate concentration (5, 20, and 50 μg mL^{-1}). The results (shown in Tables S5 and S6) indicated a similar adsorption capacity under the experimental conditions used (pH 5.5, temperature 25 °C, and 120 min of agitation).

Although no material-specific selectivity was observed under the experimental conditions, OPB was selected for PCM based on its morphological characteristics and surface charge, which may slightly favor adsorption. PPB was correspondingly selected

 © 2026 The Author(s). Published by the Royal Society of Chemistry

Open Access Article. Published on 18 May 2026. Downloaded on 5/20/2026 7:35:47 PM.
This article is licensed under a Creative Commons Attribution-NonCommercial 3.0 Unported Licence.

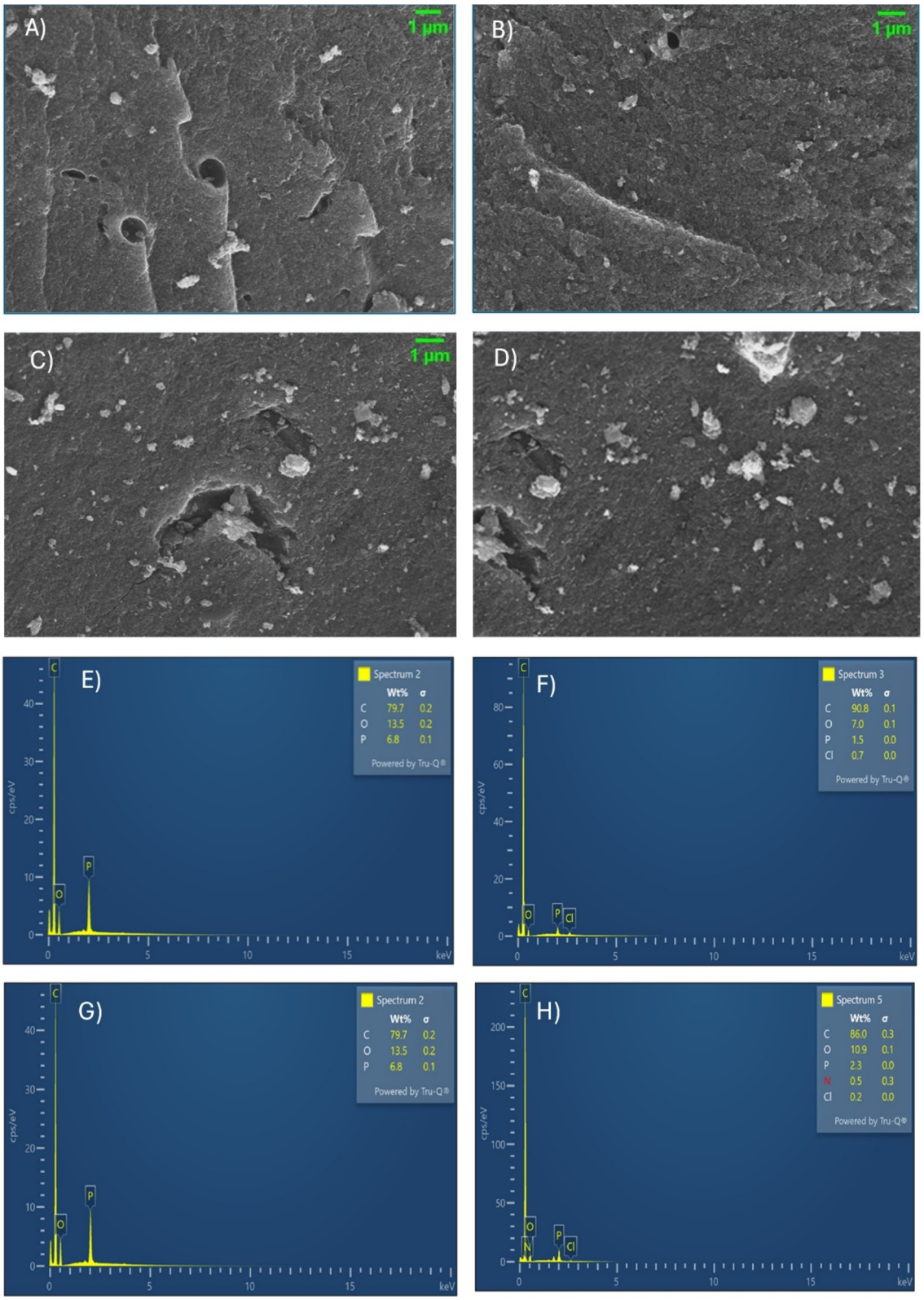

Fig. 1 SEM images, (A) and (B) before and after PCM adsorption on OPB, (C) and (D) before and after IMI adsorption on PPB. EDS spectra: (E) and (F) before PCM adsorption on OPB, (G) and (H) before and after IMI adsorption on PPB.

for IMI on practical grounds, aiming to broaden the applicability of this type of adsorbents to compounds with differing physicochemical properties.

According to the ANOVA results, the adjusted coefficient of determination for the model obtained through RSM for PCM adsorption was 0.994 with a p-value <0.001 (Table S7).

Open Access Article. Published on 18 May 2026. Downloaded on 5/20/2026 7:35:47 PM. This article is licensed under a Creative Commons Attribution-NonCommercial 3.0 Unported Licence.

Table 1 BET surface area and porosity measurement of biochar

Biochar	OPB	PPB
Specific surface area/m^2 g^{-1}	1054.2	1002.9
Total pore volume/cm^3 g^{-1}	1.14	1.21
Mesopore area/m^2 g^{-1}	700.5	732.3
Micropore area/m^2 g^{-1}	353.5	270.6
Mesopore volume/cm^3 g^{-1}	0.99	1.16
Micropore volume/cm^3 g^{-1}	0.15	0.044
Pore size/Å	43.1	48.1

Furthermore, the normal plot of residuals and the comparison between the predicted and experimental values confirmed the model accuracy and reliability. The individual effects of the adsorbent mass, the initial concentration of the adsorbate, and the initial pH were highly significant with p-values <0.001. On the other hand, the interactions between the adsorbent mass and the initial adsorbate concentration (p-value = 0.001) and the interaction between these variables with the initial pH (p-value 0.008 and 0.002, respectively) were also significant. The influence of these effects is observed in the response surface plots in Fig. 4. The highest pesticide adsorption capacity was obtained at the lowest mass of adsorbent (Fig. 4A), favored by the high concentration of PCM in solution, allowing an efficient occupation of active sites. When a greater amount of adsorbent is added, the number of active adsorption sites increases, but under the same adsorbate concentration, there are not enough molecules to occupy all the sites resulting in a lower adsorption capacity per unit mass. However, this effect could also be related to a shift in the adsorption equilibrium caused by a decrease in the concentration gradient between the bulk phase and the adsorbent, with an inefficient occupation of the active sites.[51,52] The significant interaction between pH and PCM concentration, and biochar mass is described in Fig. 4B and C. In both cases, the highest adsorption capacity of the pesticide onto the biochar was achieved under acidic pH conditions; however, this effect is more pronounced at higher concentrations of PCM, and lower amount of biochar. As was previously discussed, the negative charge of the adsorbent increases at high pH values because of the sequential deprotonation of the OH groups from H_3PO_4, and this fact could produce, in some extent, electrostatic repulsion of the deprotonated carboxyl group of PCM. However, at higher adsorbent dosages, characterized by a greater density of negative charge, the influence of pH becomes negligible; consequently, other mechanisms favoring PCM adsorption would be present. The contact time was not a significant variable in the experimental domain used (12–108 min), indicating that a rapid equilibrium is achieved predominantly by an instantaneous adsorption process. According to the model, the maximum adsorption capacity would be 51 μg mg^{-1} with a combined effect obtained at pH 2, adsorbate concentration 50 μg mL^{-1}, adsorbent mass 7.5 mg, and equilibration time 75 min. However, the maximum experimental adsorption capacities, 34.5 and 38.9 μg mg^{-1}, were obtained at the same initial concentration at pH 3.7 and 5.5, and 11.7 and 6.7 mg of adsorbent mass (Table S2), respectively, because of the interaction between all variables.

For the adsorption of IMI onto PPB, the selected variables were the adsorbent mass, the initial adsorbate concentration, and the temperature. IMI is considered as a non-ionizable compound at typical environmental pH, so this effect was not included in the study. The contact time was replaced in this test by the effect of the temperature because of the scarce effect of this variable previously described for PCM, and the similar adsorption capacity obtained for PCM and IMI on the two adsorbents in the preliminary studies. The adjusted coefficient of determination for the adsorption model was 0.996 with a p-value <0.001 (Table S8). Just like in PCM adsorption, the normal plot of residuals and the comparison between the predicted and experimental values confirmed the model accuracy and reliability. In this case, only the adsorbent mass and the initial concentration of IMI and their interaction were significant (p-value <0.001). The influence of these effects is shown in Fig. 5. The interaction effect between the first two variables can be observed in Fig. 5A. A high adsorption capacity was obtained at the lowest adsorbent mass with a slight tendency towards saturation of the active sites at the highest IMI concentration, while at the highest adsorbent mass, this capacity was strongly decreased without any tendency towards obtaining equilibrium. In Fig. 5B, the null effect of temperature can be observed, being the adsorption process mainly dependent on the concentration

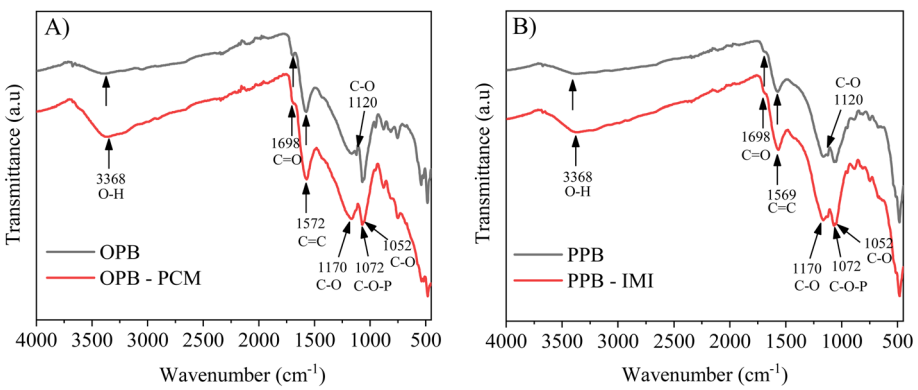

Fig. 2 FTIR spectra for (A) OPB and (B) PPB before (–) and after (–) adsorption of PCM and IMI, respectively.

© 2026 The Author(s). Published by the Royal Society of Chemistry

Open Access Article. Published on 18 May 2026. Downloaded on 5/20/2026 7:35:47 PM.
This article is licensed under a Creative Commons Attribution-NonCommercial 3.0 Unported Licence.

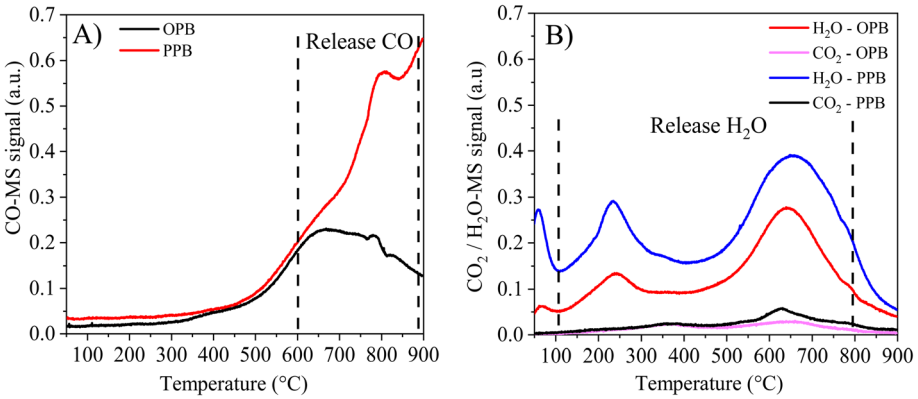

Fig. 3 TPD spectra of orange and potato peel biochars before the adsorption process: (A) CO evolution; (B) CO_2 + H_2O evolution.

of adsorbate. According to the model, the maximum adsorption capacity would be 66.2 μg mg^{-1} at the combined effect of adsorbent mass 5 mg, adsorbate concentration 50 μg mL^{-1}, and temperature 26 °C. The maximum experimental value was 52.3 μg mg^{-1} at an adsorbent mass of 7.5 mg (Table S3), the same initial concentration, and 20 °C, consistent with the interaction between the adsorbent mass and the initial concentration of IMI.

3.3 Adsorption kinetics of PCM and IMI

The effect of contact time on the adsorption of PCM and IMI is shown in Fig. 6 and 7, and the parameters obtained by fitting data to the pseudo-first order, pseudo-second-order, and intra-particle diffusion models are presented in Tables S9 and S10. Fig. 6A and 7A show that both PCM and IMI were rapidly adsorbed regardless of the initial pesticide concentration (15 and 35 μg mL^{-1}), reaching experimental adsorption capacities (q_{max}-exp) of 17.8 ± 0.4 and 33.1 ± 0.3 μg mg^{-1} for PCM, and 19.1 ± 0.4 and 41.5 ± 0.6 μg mg^{-1} for IMI, respectively. The majority of adsorption occurred within the first 10 minutes of contact (≥96% for PCM and ≥95% IMI), trending to the equilibrium with less significant changes thereafter. This is consistent with the previous behavior determined for PCM through RSM, where the contact time (12–108 min) was not

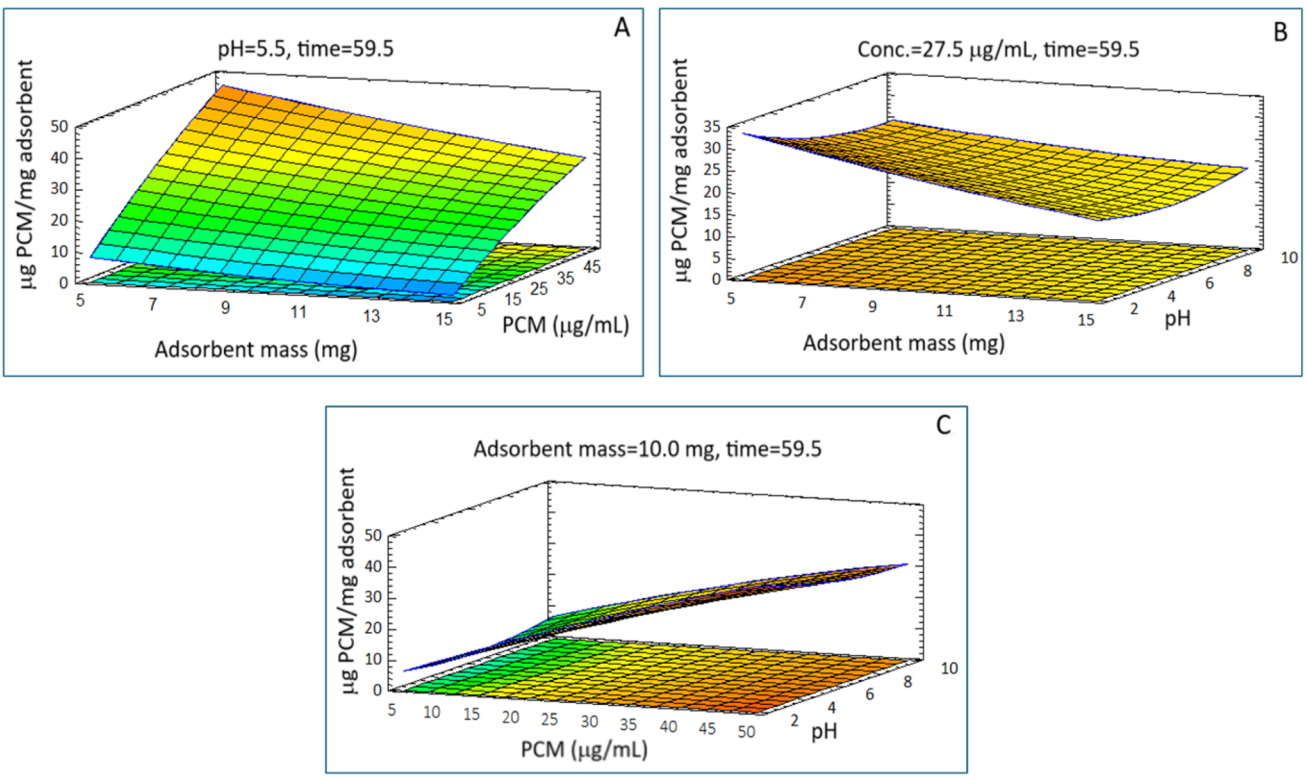

Fig. 4 Surface response plots for PCM adsorption on OPB and the significant interactions: (A) adsorbent mass and PCM concentration, (B) adsorbent mass and pH, and (C) PCM concentration and pH.

Open Access Article. Published on 18 May 2026. Downloaded on 5/20/2026 7:35:47 PM.
This article is licensed under a Creative Commons Attribution-NonCommercial 3.0 Unported Licence.

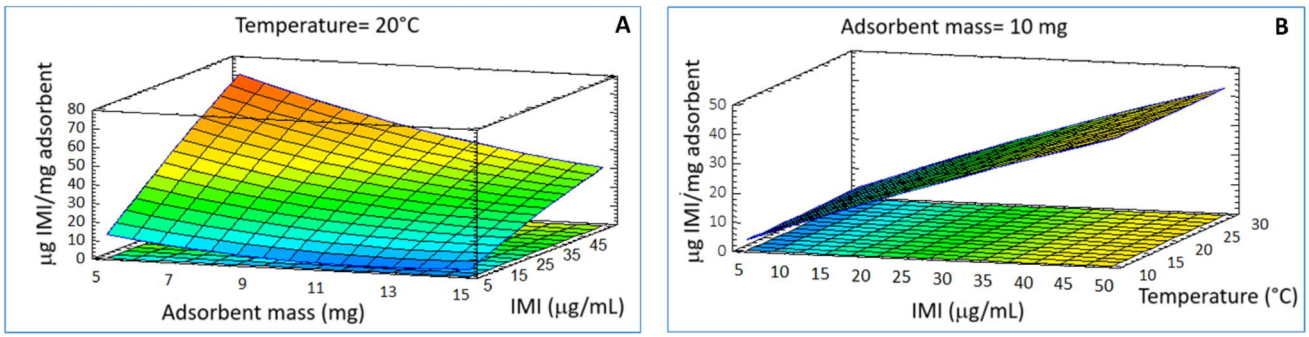

Fig. 5 Response surface plots for IMI adsorption on PPB showing the effects of: (A) adsorbent mass and IMI concentration, and (B) temperature and IMI concentration.

a significant variable. The same pattern was obtained when the adsorbent dose was varied (5 and 10 mg), keeping the analyte concentration constant (Fig. 6C and 7C), with an adsorption ≥92% in both compounds, reaching q_{max}exp values of 31.6 ± 0.3 and 22.0 ± 0.5 µg mg^{-1} for PCM and 41.6 ± 0.4 and 23.5 ± 0.8 µg mg^{-1} for IMI, respectively.

High adj R^2 values (≥0.994) and predicted adsorption capacities (q_{max}) closely aligned with the experimental ones obtained in the pseudo-second-order model in both experimental sets for the two contaminants (*e.g.*, 17.9 ± 0.06 and 32.8 ± 0.1 µg mg^{-1} for PCM and 19.1 ± 0.03 and 41.4 ± 0.1 µg mg^{-1} for IMI). By keeping the adsorbent mass constant and increasing the initial concentration of PCM and IMI, the rate constants (k_2) decreased (from 0.16 ± 0.00 to 0.073 ± 0.006 mg µg^{-1} min^{-1} for PCM and from 0.208 ± 0.01 to 0.0524 ± 0.002 mg µg^{-1} min^{-1} for IMI). On the other hand, by using a larger amount of adsorbent for the same initial concentration, higher k_2 values were observed (up to 0.145 ± 0.009 and 0.150 ± 0.01 mg µg^{-1} min^{-1} for PCM and IMI, respectively). In this model, the driving force is considered to be proportional to the available active sites (q_e–q_t);[53] consequently, the adsorbent active sites will saturate rapidly at lower initial concentrations, as well as at a larger amount of adsorbent, which will provide greater availability of active sites for the same amount of

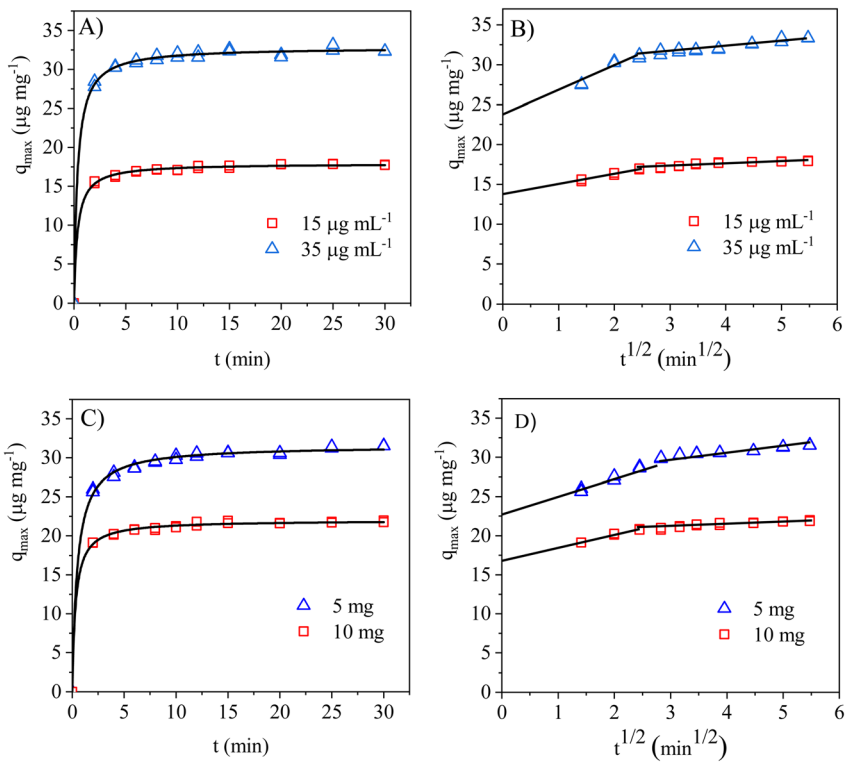

Fig. 6 Influence of the initial concentration (adsorbent mass 7.5 mg, (A) and (B)) and adsorbent mass (initial concentration 25 µg mL^{-1}, (C) and (D)) on the adsorption kinetics of PCM on OPB (n = 2). Solid lines represent the fitted data to the pseudo-second order and intraparticle diffusion models.

© 2026 The Author(s). Published by the Royal Society of Chemistry

Open Access Article. Published on 18 May 2026. Downloaded on 5/20/2026 7:35:47 PM.
This article is licensed under a Creative Commons Attribution-NonCommercial 3.0 Unported Licence.

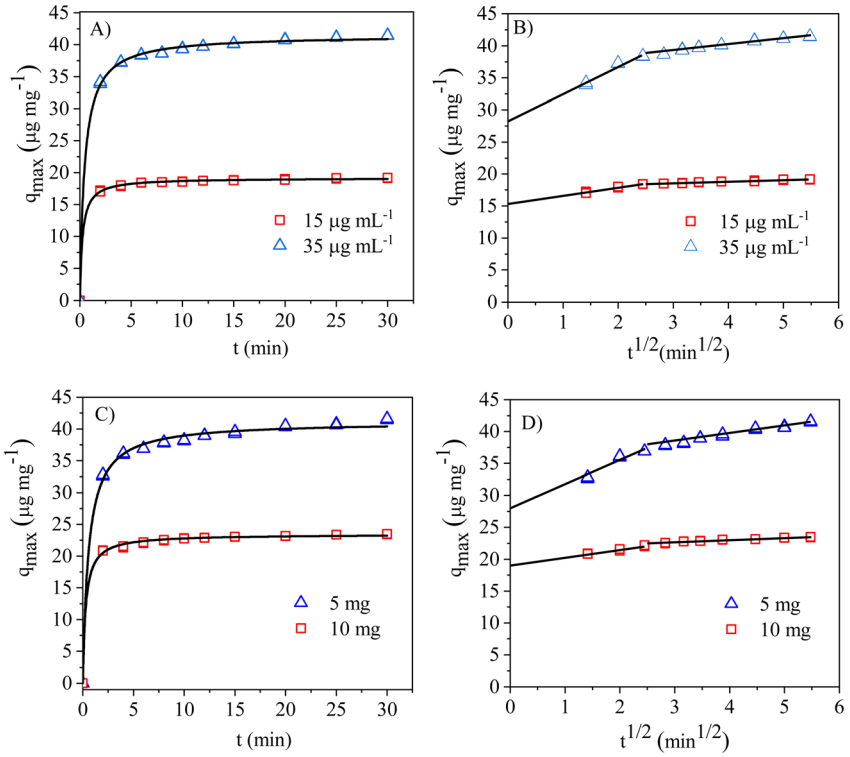

Fig. 7 Influence of the initial concentration (adsorbent mass 7.5 mg, (A) and (B)) and adsorbent mass (initial concentration 25 μg mL^{-1}, (C) and (D)) on the adsorption kinetics of IMI on PPB ($n = 2$). Solid lines represent the fitted data to the pseudo-second order and intraparticle diffusion models.

adsorbate. A good fit of the pseudo-second-order model is attributed to low initial adsorbate concentration, improved data representation during the final stages of the adsorption, and the abundance of active sites.[54] A higher abundance of different active sites and greater porosity and surface area are the main characteristics of phosphoric acid-activated biochar, which lead to improved adsorption capacities for different organic pollutants.[30] For the pseudo-second-order model, the initial adsorption rate as q_t/t approaches 0 is defined as $h = k_2 \times q(\text{max})$,[2] with calculated values ranging from 51.3 to 78.5 mg μg^{-1} min^{-1} for PCM and from 72.5 to 89.8 mg μg^{-1} min^{-1} for IMI. These values were much higher than the intrinsic constant established through the model for both compounds. This fact constitutes a preliminary antecedent to establish that in the activated biochar; there is a high initial contribution of mass-transport through the high number of vacant sites accessible for the adsorption. The pseudo-first-order model was also evaluated and provided a reasonable description of the adsorption kinetics, with adj R^2 values ranging from 0.979 to 0.991 for PCM and from 0.972 to 0.993 for IMI. However, in all cases, as mentioned above, the pseudo-second-order model showed a better agreement with the experimental data.

The internal diffusion models assume that the diffusion of adsorbate within adsorbent is the slowest step and the diffusion of adsorbate in the liquid film around the adsorbent and the adsorption onto the active sites are instantaneous.[54] The fitting of data to the intraparticle diffusion model is represented in Fig. 6B and D for PCM, and Fig. 7C and D for IMI, plots of q_t *vs.* $t_{1/2}$. When a straight line passes through the origin the intraparticle diffusion would be the controlling step; however, it did not occur. Nevertheless, data could be separated into two linear regions under both experimental sets. The parameters derived are presented in Tables S9 and S10. In all cases, the constant rate of the first stage (k_1) was higher than that of the second stage (k_2) (*e.g.*, 1.20 ± 0.09 *vs.* 0.283 ± 0.06 μg mg^{-1} min$^{1/2}$ for PCM and 1.24 ± 0.1 *vs.* 0.250 ± 0.01 μg mg^{-1} min$^{1/2}$ for IMI), and the constant values (C) calculated by linear regression analysis of data for the first stage were higher for the higher concentration of adsorbates and the lower adsorbent mass used. The constant of the model has been related to the boundary layer effect, and this effect would be greater as the constant value increases.[54,55] Therefore, the overall adsorption process is primarily governed by the high density of active sites and external film diffusion, though intraparticle diffusion into internal pores also provides a significant contribution for both adsorbents.

The kinetic behavior of IMI adsorption on PPB, compared to that obtained for a non-activated eucalyptus wood biochar, under similar experimental conditions,[56] indicated significantly higher kinetic constants for the pseudo-first and pseudo-second order kinetic models, as well as shorter equilibrium times, with a clear contribution from instantaneous adsorption on the active sites. This improved kinetic performance is attributable to the higher number and accessibility of active sites, which facilitate more efficient interactions with the adsorbent.

© 2026 The Author(s). Published by the Royal Society of Chemistry

Open Access Article. Published on 18 May 2026. Downloaded on 5/20/2026 7:35:47 PM. This article is licensed under a Creative Commons Attribution-NonCommercial 3.0 Unported Licence.

3.4 Adsorption isotherms of PCM and IMI

The isotherm parameters obtained by fitting the experimental data to the Freundlich, Langmuir, and Dubinin–Radushkevich models are presented in Table 2 and Fig. 8, respectively. Given the results obtained from the optimization of variables influencing the adsorption process of IMI onto PPB, where temperature effect was not significant, the adsorption was only conducted at 25 °C. Data for PCM on OPB at 15, 25, and 35 °C, and IMI on PPB at 25 °C fitted better to the Freundlich model with R_{adj}^2 values ≥0.99. This result suggests that PCM and IMI adsorption on the activated biochars preferentially occur on a heterogeneous surface containing the adsorption sites, as observed in the SEM images (Fig. 1A and B), through a multilayer mechanism. The parameter $1/n$ for PCM adsorption ranged from 0.300 ± 0.08 to 0.319 ± 0.07, whereas for IMI it was 0.319 ± 0.01. Values <0.5 indicate easy adsorption and heterogeneous energetic distribution of active sites.[57] On the other hand, the K_F value was higher for IMI adsorption in agreement with the adsorption capacity shown through RSM and kinetic results for both compounds. Lower adjusted R^2 values were obtained when fitting the data to the Langmuir model (0.93–0.95 for PCM and 0.98 for IMI). As shown in Fig. 8, both compounds exhibit only a tendency toward saturation of the active sites; therefore, the predicted q_{max} values are likely higher than those observed at the maximum initial concentration evaluated. Despite the lower R_{adj}^2 associated with this model, the K_L constant was higher for IMI, indicating a more favorable adsorption–desorption equilibrium, as this parameter reflects the ratio between adsorption and desorption rates at equilibrium.[58]

The Dubinin–Radushkevich model has been extensively used in liquid–solid adsorption systems to determine whether the adsorption was dominated by physical or chemical processes *via* calculating the associated mean free energy (kJ mol^{-1}). However, recent publications reported that the Polanyi potential (ε, kJ mol^{-1}) was often incorrectly calculated, affecting the estimation of the model parameters (K_{DR}, and Q_{max}, maximum adsorption capacity).[57,58,68–70] According to the above, the model parameters were calculated by evaluating the modifications proposed in the literature. The data were well fitted to this model (adj R^2 0.969–0.999), with predicted maximum adsorbed values more consistent with the saturation trend observed in Fig. 8, for both contaminants. The mean free energy (E) calculated for the adsorbents were <8 kJ mol^{-1}, indicating a physical adsorption for both compounds.

The activated biochar used for IMI showed a high adsorption capacity compared to other unmodified biochars produced under different conditions. For example, K_F values between 0.18 and 1.7 have been reported for biochar derived from various plant residues pyrolyzed at 600 °C.[59] The best performance was obtained with a rice straw-derived biochar, which was the most porous adsorbent (pore volume = 0.646 cm^3 g^{-1}), and had a surface area of 220 m^2 g^{-1}. This biochar was further modified by using H_3PO_4 after the pyrolysis, resulting in a K_F value of 3.2,

Table 2 Isotherm model parameters for PCM on OPB and IMI on PPB at different temperatures ($n = 2$)

		Temperature		
Model	Parameters	15 °C	25 °C	35 °C
PCM-OPB				
Langmuir	q(exp)[a] (μg mg^{-1})	38.5 ± 0.4	36.3 ± 0.8	35.9 ± 0.4
	q_{max} (μg mg^{-1})	38.9 ± 1.3	37.2 ± 1.2	37.0 ± 1.4
	K_L (mL μg^{-1})	0.51 ± 0.07	0.50 ± 0.07	0.42 ± 0.07
	R_{adj}^2	0.947	0.948	0.929
Freundlich	$1/n$	0.309 ± 0.09	0.300 ± 0.08	0.319 ± 0.07
	K_F ($\mu g^{1-1/n}$ $mL^{1/n}$ mg^{-1})	14.9 ± 0.3	14.5 ± 0.3	13.4 ± 0.2
	R_{adj}^2	0.990	0.990	0.994
D–R	q_{max} (μg mg^{-1})	42.2 ± 0.7	40 ± 0.5	39 ± 0.6
	K_{D-R} (mol^2 J^{-2}) ($\times 10^{-9}$)	9.5 ± 0.4	8.7 ± 0.4	8.7 ± 0.6
	E (kJ mol^{-1})	7.2	7.6	7.6
	R_{adj}^2	0.984	0.987	0.969
IMI-PPB				
Langmuir	q_{max}(exp) (μg mg^{-1})	—	51.5 ± 0.6	—
	q_{max} (μg mg^{-1})	—	52.8 ± 1.3	—
	K_L (mL μg^{-1})	—	1.00 ± 0.09	—
	R_{adj}^2	—	0.980	—
Freundlich	$1/n$	—	0.319 ± 0.01	—
	K_F ($\mu g^{1-1/n}$ $mL^{1/n}$ mg^{-1})	—	24.6 ± 0.5	—
	R_{adj}^2	—	0.991	—
D–R	q_{max} (μg mg^{-1})	—	56.0 ± 0.3	—
	K_{D-R} (mol^2 J^{-2}) ($\times 10^{-9}$)	—	7.4 ± 0.1	—
	E (kJ mol^{-1})	—	8.2	—
	R_{adj}^2	—	0.999	—

[a] q(exp) corresponds to the adsorbed amount of the adsorbate at the highest initial concentration employed.

© 2026 The Author(s). Published by the Royal Society of Chemistry

Open Access Article. Published on 18 May 2026. Downloaded on 5/20/2026 7:35:47 PM.
This article is licensed under a Creative Commons Attribution-NonCommercial 3.0 Unported Licence.

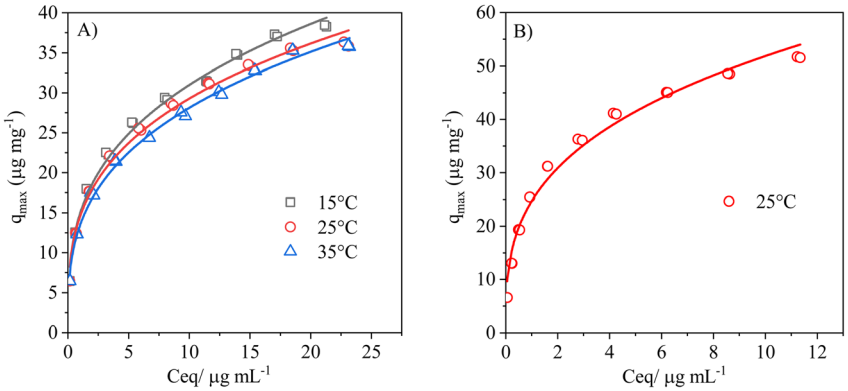

Fig. 8 Isotherm plots for: (A) PCM adsorption on OPB at 15, 25, and 35 °C and (B) IMI adsorption on PPB at 25 °C (B) ($n = 2$). Solid lines represent the fitted data to the Freundlich model.

although this treatment reduced both surface area and pore volume. Similarly, K_F constants of the same order of magnitude as those obtained for IMI adsorption on PPB have been reported for a maize straw-derived biochar modified by a deep deashing treatment but using 100 mg of adsorbent.[60] For PCM, higher adsorption was obtained for an aged oak wood-derived biochar (incubated for six months in a silt loam soil) compared to the fresh biochar;[61] however, the distribution coefficients (K_d) value was still significantly lower than that obtained for PCM adsorption on OPB. On the other hand, high adsorption capacities were observed at pH 2 for other two phenoxyacids, 2,4-D and MCPA (28 and 79 µg mg^{-1}), but using 25 mg of biochar and considerably higher adsorbate concentrations (300 and 100 µg mL^{-1}), respectively.[62]

As was observed in the RSM results, PCM presented a significant adsorption at an initial pH of 3. In this condition, PCM remained partially protonated (neutral) and the negative electrostatic interaction with the anionic species will be reduced because the zeta potential values of OPB at this pH was less negative (−8.4 mV). These conditions, together with the significant microporous fraction of the adsorbent (~30%), suggest that pore-filling processes may also play an important role. The gradual decrease at higher pH, although adsorption remained significant under neutral conditions, indicated that electrostatic interactions are not the sole controlling factor. The zeta potential reflects the potential at the shear plane rather than the chemical state of surface functional groups. The PCM molecule contains four hydrogen bond acceptor groups (pyridinic nitrogen, amino group, and oxygen atoms in the carboxyl group), indicating that hydrogen bonding with OH and phosphate groups on the adsorbent surface may also contribute to the adsorption process.[48] Conversely, the contribution of π–π interactions with the OPB surface, suggested for other phenoxy acids on biochars,[62] is likely limited in this case, as the electron density of the aromatic ring is reduced by the presence of three chlorine atoms in the PCM structure. Hydrogen-bonding is a short-range, directional, and site-specific interactions unlike long-range electrostatics. Hydrogen bonding can locally overcome electrostatic repulsion, especially within the confined environment of biochar micropores, where the effective interaction distance is reduced and charge influence is enhanced. This observation is consistent with the isotherm results, which were better described by the Freundlich isotherm model, suggesting a heterogeneous surface with multiple types of adsorption sites. Furthermore, the adsorption kinetics followed the pseudo-second-order kinetics model, indicating that the rate-limiting step is associated with specific interactions rather than simple mass transfer. In addition, the intraparticle diffusion analysis suggested that pore diffusion contributes to the overall adsorption mechanism, consistent with the presence of microporous in the structure of the activated biochar. Overall, these results demonstrate that PCM adsorption is governed by a combination of surface heterogeneity, specific intermolecular interactions, and pore-filling effects, rather than purely electrostatic forces.

In contrast, the IMI adsorption does not depend on the pH of the equilibrium solution. The higher adsorption capacity observed for IMI, compared to PCM, could be explained by pore-filling processes and the presence of a greater number of hydrogen bond acceptor groups (such as the nitrogen of the pyridine ring, the amino group and the imidazole ring, in addition to the oxygens of the nitro group), which promotes its interaction with hydroxyl from aliphatic alcohols, phenols, and phosphate groups present on the surface of PPB. However, the possibility of π–π interactions between the aromatic rings of IMI and those present on the biochar surface, and the less hydrophobic nature can also explain a greater adsorption.[30,60]

3.5 Adsorption thermodynamics for PCM

The experimental data showed a good fit for the Langmuir model ($R^2 = 0.93$–0.95), supporting the use of the constant K_L as an apparent equilibrium parameter to estimate the thermodynamic properties of the system. Because this constant is not dimensionless, it was converted to the thermodynamic form by multiplying by a standard concentration of 1 mg L^{-1}, resulting in a dimensionless equilibrium constant.[71] The calculated enthalpy change ($\Delta H^\circ = -7.2$ kJ mol^{-1}) indicated that the adsorption process is exothermic, and its low magnitude reflects a weak adsorbate–adsorbent interactions. The negative

Open Access Article. Published on 18 May 2026. Downloaded on 5/20/2026 7:35:47 PM. This article is licensed under a Creative Commons Attribution-NonCommercial 3.0 Unported Licence.

entropy change ($\Delta S^\circ = 30.3$ J mol^{-1} K^{-1}) represents a decrease in randomness at the solid–solution interface during adsorption, in accordance with the adsorption of PCM onto the adsorbent surface. The ΔG° values of PCM adsorption obtained from the K_L were: +1.61 (15 °C), +1.72 (25 °C), and +1.22 (35 °C). The relatively small variation of the Langmuir constant with temperature (0.51–0.42 mL μg^{-1}) indicated a weak dependence of the adsorption equilibrium on thermal effects. Accordingly, the calculated values are low and slightly positive, indicating that the system operates close to thermodynamic equilibrium. This behavior is consistent with a weak, physisorption-driven mechanism, where adsorption and desorption processes occur simultaneously.

3.6 Desorption study

Fig. 9 shows the adsorbed amounts of PCM on OPB (A) and IMI on PPB (B) and the desorbed amounts during each desorption step at two initial adsorbate concentrations, 10 and 20 μg mL^{-1}. In the case of PCM, the cumulative desorption percentages reached 14% and 34%, while for IMI, they were significantly lower, 2% and 4%, respectively. These results could be associated with the K_L values, indicating a low ratio between the adsorption and desorption rates at equilibrium for PCM and stronger interactions for IMI, as described previously.

3.7 Adsorption of PCM and IMI on soils amended with biochar

This experiment evaluated the possible soil matrix influence on biochar's adsorption capacity and the feasibility to add them as an amendment to enhance the adsorption capacity of soils. As shown in Tables 2 and 3, the unamended soils exhibited very low or negligible adsorption capacity as reflected by the low K_d values. In the case of PCM, the limited adsorption could be attributed to the pH of soils, slightly acid or neutral, regardless of their organic matter content.[7,8] Ultisols (MET and COLL) are rich in Fe and Al oxides as well as kaolinite, presenting a moderate to near neutral point of zero charge (PZC) values. Consequently, under acidic conditions, their surfaces can approach neutrality, allowing a potential anion retention. In contrast, Mollisols are dominated by 2 : 1 clay mineral (such as smectite) which confer a low PZC (~2–3) and a predominance of permanent negative charge. Therefore, at natural soil pH values, negative electrostatic interactions with anionic species prevent their adsorption. On the other hand, for IMI, the low adsorption capacity was consistent with the K_d values observed in soils with low organic matter content.[11,12,63]

Soil matrices substantially influenced the adsorption capacity of PCM on OPB (Table 3), particularly in the OLV soil, where it decreased from an average of 20 to 4.5 μg mg^{-1} (calculated as the difference between the total amount adsorbed and the amount adsorbed by unamended soils). For MET and COLL soils, the adsorption capacity decreased to an average of 8.1 and 9.4 μg mg^{-1}. Based on the previous background, the greater matrix effect in OLV soil can be explained by the dominant effect of the soil's permanent negative charge, which is added to the negative charge of the adsorbent at the system's pH (6.9). Conversely, this effect is unlikely in MET and COLL soils. On the other hand, the adsorption capacity of PCM on OLV soil was appreciable, suggesting that surface charge-independent interactions, previously discussed, persist even in the presence of the soil matrix. The matrix effect observed for MET and COLL soils, with an adsorbent capacity independent of the added mass, may be due to compounds in the soil solution that compete with PCM for the active sites during the adsorption process. Despite the influence of the soil matrix, a significant improvement in adsorption capacity was obtained in all soils with the highest amount of OPB. Specifically, for the unamended MET and COLL soils, the adsorbed amounts were 8% and 12% of the initial amount of adsorbate in solution, respectively, while for the amended soils, they were 49% and 41%, respectively.

The decrease in IMI adsorption on PPB due to the soil matrix was much less pronounced, including the OLV soil. In this case, the lower PPB adsorption capacity with increasing adsorbent mass was observed in all soils (Table 4), which agrees with the results obtained through RSM. In the amended soils, the K_d values increased on average 31, 75, and 128 times with the addition of increasing amounts of adsorbent compared to those of the unamended soils, with the best results obtained for MET soil. Consequently, higher adsorption rates (≥80% in the MET and COLL soils and 77% in the OLV soil) were obtained. It can be noted that these increased adsorption capacities were obtained by using a low dose of soil amendment (0.25–0.5%)

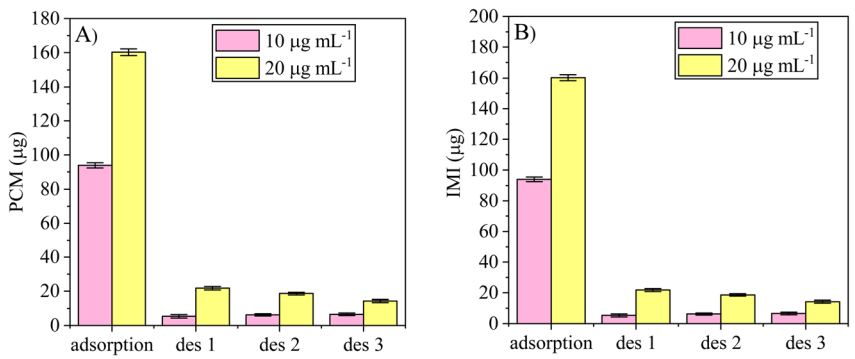

Fig. 9 Desorption of PCM from OPB (A) and IMI from PPB (B), at two initial concentrations (mean values of duplicates).

© 2026 The Author(s). Published by the Royal Society of Chemistry

Open Access Article. Published on 18 May 2026. Downloaded on 5/20/2026 7:35:47 PM. This article is licensed under a Creative Commons Attribution-NonCommercial 3.0 Unported Licence.

Table 3 Influence of the soil matrix on the adsorption of PCM on OPB and adsorption capacity of amended soil (initial concentration 25 μg mL^{-1}, $n = 2$)

Soil/biochar	Added OPB (mg)	Soil adsorption (μg g^{-1})	OPB adsorption (μg mg^{-1})	K_d (mL g^{-1})	% Adsorbed
Metrenco	—	9.9 ± 1.1	—	0.4 ± 0.05	8
Collipulli	—	14.6 ± 0.6	—	0.7 ± 0.07	12
Olivar	—	0.4 ± 0.1	—	0.0 ± 0.0	0.3
OPB	5	—	20.5 ± 0.3	—	42
	7.5	—	21.8 ± 0.3	—	67
	10	—	19.1 ± 0.1	—	77
Metrenco	5	29.3 ± 2.2	7.8 ± 0.3	1.5 ± 0.2	23
	7.5	40.9 ± 0.7	8.3 ± 0.2	2.4 ± 0.01	33
	10	50.7 ± 0.6	8.2 ± 0.07	3.4 ± 0.06	41
Collipulli	5	38.1 ± 1.3	9.4 ± 0.3	2.2 ± 0.1	30
	7.5	50.7 ± 1.1	9.6 ± 0.1	3.4 ± 0.1	41
	10	60.2 ± 0.8	9.1 ± 0.2	4.7 ± 0.1	49
Olivar	5	9.5 ± 1.1	3.7 ± 0.2	0.4 ± 0.06	8
	7.5	19.2 ± 1.2	5.0 ± 0.2	0.9 ± 0.08	15
	10	24.2 ± 0.3	4.8 ± 0.1	1.2 ± 0.02	20

compared to those used with an optimized unmodified biochar (1–20%) for which the increase varied between 5 and 120 times the soil K_d value.[64]

3.8 Transport of PCM and IMI

These experiments were conducted to assess the ability of biochars to prevent or reduce the vertical transport through soils with low K_d values for both compounds. The resulting breakthrough curves (BTC) which represent the amount eluted in each fraction relative to the total amount of adsorbate added (Q/Q_0) *vs.* the relative pore volume (V/V_0), are shown in Fig. 10 and 11 for PCM and IMI, respectively. The results are also presented in Table S11. The elution of ^3H_2O in Metrenco and Collipulli soils began at about 0.5 PV and in Olivar soil at 0.8 PV. A slight asymmetrical elution was observed for Metrenco and Olivar soils, and the maximum amount in the eluates was reached close to 1 in all cases. This behavior is consistent with physical equilibrium in all soils, so water does not tend to stagnate (Fig. S4).

Related to the mobility of PCM, different results were obtained in soils. In amended Olivar, Metrenco, and Collipulli soils, at least 1.3, 1.5, and 2.1 PV were required to initiate the elution, reaching a maximum at 1.8, 2.5, and 3 PV, respectively. The displacement of the retardation factors compared to the ^3H_2O indicated that a fraction of PCM was adsorbed, particularly for Metrenco and Collipulli soils. However, it was slowly desorbed, producing a high accumulative recovery in the eluates at 5 PV for all soils (93–95%, Table S11). These results agree with the K_d values determined in the previous study. Overall, the results showed relatively rapid leaching in all soils under study. Considering the soil matrix effects, it was decided

Table 4 Influence of the soil matrix on the adsorption of IMI on PPB and adsorption capacity of amended soil (initial concentration 25 μg mL^{-1}, $n = 2$)

Soil/biochar	Added PPB (mg)	Soil adsorption (μg g^{-1})	PPB adsorption (μg mg^{-1})	K_d (mL g^{-1})	% Adsorbed
Metrenco	—	14.8 ± 0.2	—	0.7 ± 0.07	12
Collipulli	—	21.0 ± 0.8	—	1.0 ± 0.05	17
Olivar	—	22.8 ± 0.5	—	1.1 ± 0.02	19
PPB	5	—	44.5 ± 0.1	—	89
	7.5	—	31.7 ± 0.1	—	95
	10	—	24.1 ± 0.07	—	96
Metrenco	5	106.1 ± 0.6	36.5 ± 0.3	28.1 ± 0.4	73
	7.5	116.4 ± 0.2	27.1 ± 0.1	68.0 ± 1.1	81
	10	120.3 ± 0.07	21.1 ± 0.07	126.7 ± 1.4	84
Collipulli	5	108.5 ± 0.4	35.0 ± 0.4	32.9 ± 0.7	70
	7.5	117.5 ± 0.07	25.7 ± 0.2	77.9 ± 0.2	77
	10	120.0 ± 0.07	19.8 ± 0.2	120.1 ± 1.3	79
Olivar	5	104.0 ± 0.9	32.5 ± 0.5	24.8 ± 1.1	65
	7.5	114.5 ± 0.2	24.4 ± 0.07	54.4 ± 1.1	73
	10	119.3 ± 0.07	19.3 ± 0.2	104.7 ± 0.6	77

Open Access Article. Published on 18 May 2026. Downloaded on 5/20/2026 7:35:47 PM.
This article is licensed under a Creative Commons Attribution-NonCommercial 3.0 Unported Licence.

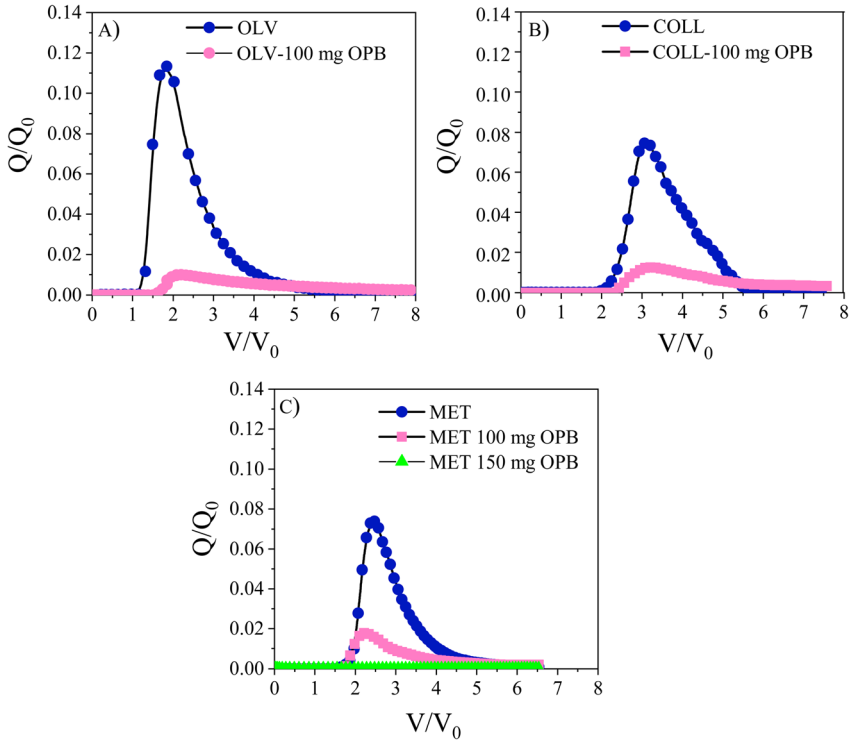

Fig. 10 Breakthrough curves of PCM transport in amended and unamended soil columns ($n = 2$).

to add 150 mg of OPB mixed with 1 g of soil as a retention barrier in the Metrenco soil, resulting in a 100% adsorption (Fig. 10C). According to this result, the adsorbent dose was reduced to 100 mg to compare its behavior in the three soils. Despite the higher matrix effect observed previously for the Olivar soil, the maximum height in the BTC was lower than that

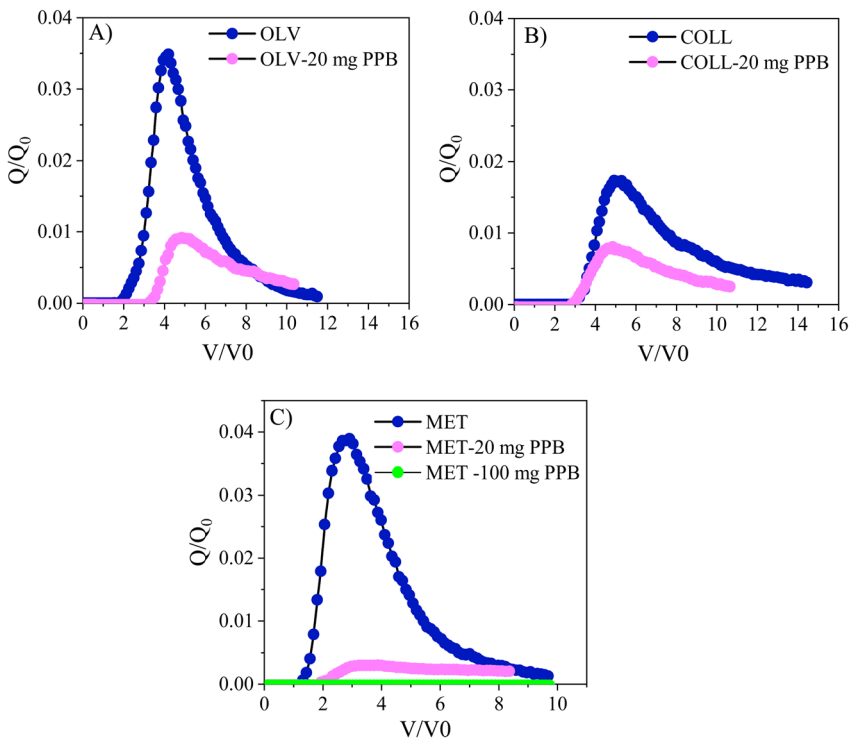

Fig. 11 Breakthrough curves of IMI transport in amended and unamended soil columns ($n = 2$).

© 2026 The Author(s). Published by the Royal Society of Chemistry

Open Access Article. Published on 18 May 2026. Downloaded on 5/20/2026 7:35:47 PM. This article is licensed under a Creative Commons Attribution-NonCommercial 3.0 Unported Licence.

obtained for the other two soils. The scarce effect of the soil matrix could be due to the higher number of active sites, according to the higher mass of adsorbent used as a barrier. Furthermore, the eluted amount at 5 PV and the retained % at the end of the elution (6.5–8 PV) were similar for all soils (70–74%).

For IMI, at least 1.3, 1.9, and 3 pore volumes were required to initiate compound elution for amended Metrenco, Olivar, and Collipulli soils, respectively. The maximum height of the BTC was obtained at 2.6, 4.2, and 5.3 PV, and at the end of the elution, the total amount recovered in the eluates reached 94, 86, and 74% (Table S11). The mobility of IMI in soil columns could be attributed to the K_d values determined previously; however, a significant slower desorption was observed for Collipulli soil (Fig. 11B), reaching an elution of 60% of the added amount at 10 PV. At the same PV, 94 and 85% were eluted for Metrenco and Olivar soil. A preliminary test was also conducted by using 100 mg of PPB as amendment in the Metrenco soil column, but the compound was undetectable in all the eluates (Fig. 11C). Given the greater adsorption capacity demonstrated for this adsorbent and the lower effect of soil matrix compared to PCM, the following experiments were conducted by using 20 mg. The effect of PPB adsorbent was highly effective, significantly lowering the maximum height of the BTC, particularly in the Olivar and Metrenco soil. The slow desorption in the amended Collipulli soil was also observed. Due to the initial elution delay of IMI, the comparison with the behavior in amended soils was conducted by using as a reference the total elution at 8.5 PV. The amounts eluted were 24% for Collipulli and Olivar soils, and 12% for the Metrenco soils. Consistent with the low desorption rate and the low effect of soil matrices on the adsorption capacity of PPB, the behavior observed in the amended soils could be mainly attributed to the interactions between IMI and soil components.

According to the results obtained, a total immobilization could be reached for PCM and IMI with a slightly higher amount of amendment under the same experimental conditions. Furthermore, a higher dose of the adsorbent would allow to reduce possible effects of the matrix of different soils, as was observed specially for PCM.

Different studies have proposed the use of biochars to amend soils with remediation purposes or to avoid leaching of organic contaminants. For instance, the addition of unmodified biochar doses ≥5% resulted in a higher adsorption of imidacloprid, clothianidin, isoproturon, metolachlor, and atrazine on amended soils.[63–65] Likewise, successful stabilization of six per- and polyfluoroalkyl substances (PFAS) in field-contaminated soils was achieved by using activated biochars. The leaching was reduced to 23–100% and >90% at an application dose of 5% and 1–5% for a soil with high and low total organic carbon, respectively.[66] All these results were obtained in batch experiments. Similar results were reported for column leaching tests in a contaminated soil amended with 1% of de-watered sludge, with a leaching reduction of 80–100% for perfluoroalkyl sulfonates and between 60–80% for perfluorocarboxylic acids with activated waste timber biochar.[67]

The present study confirmed the great potential of phosphoric acid-activated biochar to be used as an effective vertical barrier preventing the transport of PCM and IMI along the soil profile by using a low dose mixed with a small amount of soil. The results also suggest that low doses could be used to stabilize both compounds in larger volumes of contaminated soil.

4. Conclusions

The improved physical and chemical properties of phosphoric acid-activated biochar from orange and potato peels (high specific surface area, mesopore structure, high porosity, and abundance of functional groups) resulted in significant adsorption capacity for PCM and IMI. Despite the unfavorable negative charge of adsorbents, the weak acid PCM was adsorbed under environmentally relevant pH conditions (3–10). H-bonding was likely the most important adsorption mechanism due to the presence of hydrogen bond acceptor groups in both molecules, which can interact with the hydroxyl functional group in aliphatic alcohols, phenols, and phosphate groups from both biochars. However, for IMI, the greater number of hydrogen bond acceptor groups, the possibility of π–π interactions, and the less hydrophobic nature explain its greater adsorption.

The instantaneous adsorption on active sites, with high kinetic constants, along with the low desorption rates observed after three successive extraction steps (14–34% for PCM and 2–4% for IMI) ensures an effective process and suggests a long-term retention of both compounds, preventing their migration through the soil profile. On the other hand, the limited effect of temperature and pH enhances the applicability of both adsorbents under field conditions.

The influence of soil matrices on the adsorption capacity of biochars was most pronounced for PCM, particularly in the non-volcanic soil. In volcanic soils, however, the incorporation of a low-dose amendment (0.5%) enhanced the K_d value by up to eightfold. In contrast, the reduced matrix interferences observed for imidacloprid led to an average 117-fold increase in the K_d value across all soils.

Amendment of soils with little or no capacity to adsorb PCM and IMI by using a low-dose biochar barrier added to 100 g soil columns (20 mg for IMI and 100 mg for PCM mixed with 1 g of soil) proved to be highly effective, limiting leaching to 25–30% and 12–24%, respectively, depending on the soil type. As was demonstrated, a 0% leaching can be obtained with slightly higher doses for both compounds.

These results show that biochar obtained from agricultural waste is a sustainable and effective alternative for mitigating pesticide contamination of soil and groundwater, representing a promising tool for remediation strategies in agricultural soils. Future research should focus on evaluating the long-term retention capacity of biochar amendments under different environmental conditions and exploring their functionalization for the development of reactive barriers capable of combining adsorption with the *in situ* degradation of both pollutants.

Open Access Article. Published on 18 May 2026. Downloaded on 5/20/2026 7:35:47 PM. This article is licensed under a Creative Commons Attribution-NonCommercial 3.0 Unported Licence.

Conflicts of interest

There are no conflicts to declare.

Data availability

All data supporting the findings of this study are available within the paper and supplementary information (SI). Supplementary information: additional experimental and analytical information supporting the findings of this study, including the soil column transport setup, zeta potential measurements, breakthrough curves of tritium, pesticide properties, optimization data obtained through Doehlert experimental designs, calibration and validation parameters of the analytical methods, adsorption kinetic modeling results, and transport experiments conducted in agricultural soils with and without biochar amendments. See DOI: https://doi.org/10.1039/d5ra08466k.

Acknowledgements

This work was financially supported by ANID (Agencia Nacional de Investigación y Desarrollo, Chile): Projects FONDECYT No. 11230564, Projects JUV_INVESTIGADORA_DICYT_USA21991, Código 022442VF_JUVI, Vicerrectoría de Investigación, Innovación y Creación. Universidad de Santiago de Chile, USACH, and Proyecto UTM1999 (IDT-UTEM).

References

1 Department of Economic and Social Affairs, World Population Prospects, 2024.
2 I. Berni, A. Menouni, I. El Ghazi, L. Godderis, R.-C. Duca and S. E. Jaafari, *Environ. Pollut.*, 2021, **276**, 116638.
3 M. J. Climent, E. Herrero-Hernández, M. J. Sánchez-Martín, M. S. Rodríguez-Cruz, P. Pedreros and R. Urrutia, *Environ. Pollut.*, 2019, **251**, 90–101.
4 I. F. Farah, C. R. dos Santos, M. C. F. Pinto, C. R. Araújo and M. C. S. Amaral, *J. Environ. Chem. Eng.*, 2024, **12**, 114072.
5 R. E. Barros, M. M. Reis, W. G. Montes, É. M. G. Lopes, F. F. Figueiredo and L. D. T. Santos, *Environ. Technol. Innovation*, 2021, **23**, 101682.
6 L. Gaona, F. Bedmar, V. Gianelli, A. J. Faberi and H. Angelini, *Int. J. Environ. Sci. Technol.*, 2019, **16**, 6657–6670.
7 K. E. Hall, C. Ray, S. J. Ki, K. A. Spokas and W. C. Koskinen, *J. Environ. Manage.*, 2015, **159**, 227–234.
8 G. Palma, M. Jorquera, A. Ladino, C. Benimeli and G. Briceño, *Agronomy*, 2024, **14**, 1617.
9 G. Palma, A. Sánchez, Y. Olave, F. Encina, R. Palma and R. Barra, *Chemosphere*, 2004, **57**, 763–770.
10 D. Broznic and C. Milin, *J. Environ. Sci. Health, Part B*, 2012, **47**, 779–794.
11 Y. Li, Y. D. Li, G. H. Bi, T. J. Ward and L. Li, *Environ. Sci. Pollut. Res.*, 2023, **30**, 47516–47526.
12 P. Majee and P. H. P. Reddy, *Int. J. Environ. Anal. Chem.*, 2023, **104**(20), 8570–8584.
13 G. J. Goedjen, P. D. Capel, J. D. Barry and W. A. Arnold, *Sci. Total Environ.*, 2024, **954**, 176411.
14 X. P. He, J. H. Chen, M. Xin, T. Z. Han, Y. N. Wang, C. Han and B. D. Wang, *J. Hazard. Mater.*, 2024, **477**, 135297.
15 R. Karim, L. Reading, L. Dawes, O. Dahan and G. Orr, *Soil*, 2023, **9**, 381–398.
16 D. A. Thompson, D. W. Kolpin, M. L. Hladik, K. K. Barnes, J. D. Vargo and R. W. Field, *Sci. Total Environ.*, 2021, **782**, 146762.
17 H. Wang, W. Lei, M. Wu, J. Guo, S. He, N. Shen, C. Li and L. Wang, *Environ. Pollut.*, 2025, **378**, 126507.
18 L. M. Addy-Orduna, M. E. Ortiz-Santaliestra, F. Mougeot, P. Bolívar-Muñoz, P. R. Camarero and R. Mateo, *Environ. Sci. Technol.*, 2024, **58**, 13217–13225.
19 N. W. Thunnissen, L. S. Lautz, T. W. G. van Schaik and A. J. Hendriks, *Chemosphere*, 2020, **254**, 126604.
20 C. Vignet, T. Cappello, Q. G. Fu, K. Lajoie, G. De Marco and C. Clérandeau, *Chemosphere*, 2019, **225**, 470–478.
21 J. X. Wu, P. Z. Yu, Z. Y. Zou, E. R. Zhao, J. J. Jing, J. W. Zhang, Y. Tao and L. R. Ren, *Molecules*, 2025, **30**(8), 1803.
22 Z. M. Yu, X. F. Li, S. R. Wang, L. Y. Liu and E. Y. Zeng, *Environ. Pollut.*, 2021, **284**, 117358.
23 H. Y. Zhang, M. Zhang, H. L. Zhang, X. F. Shen, W. G. Lv, X. L. Wang, J. Q. Zhang and X. Y. Guo, *Environ. Toxicol. Pharmacol.*, 2024, **111**, 104570.
24 M. Riero, G. Pereira, D. Olsson, R. Lajmanovich and R. Maneyro, *Rev. Int. Contam. Ambiental*, 2024, **40**, 533–542.
25 A. Zöngnr and M. Sari, *Biol. Futura*, 2023, **74**, 171–182.
26 M. Cycón, A. Markowicz, S. Borymski, M. Wójcik and Z. Piotrowska-Seget, *J. Environ. Manage.*, 2013, **131**, 55–65.
27 J. A. Senabio, R. C. da Silva, D. G. Pinheiro, L. G. de Vasconcelos and M. A. Soares, *PLoS One*, 2024, **19**(11), e0314492.
28 Y. Liu, L. Lonappan, S. K. Brar and S. Yang, *Sci. Total Environ.*, 2018, **645**, 60–70.
29 G. Chu, J. Zhao, Y. Huang, D. D. Zhou, Y. Liu, M. Wu, H. B. Peng, Q. Zhao, B. Pan and C. E. W. Steinberg, *Environ. Pollut.*, 2018, **240**, 1–9.
30 R. Li, C. Zhang, J. Hui, T. Shen and Y. Zhang, *Sci. Total Environ.*, 2024, **917**, 170198.
31 C. Guo, F. Hua, P. Chen, X. Wang, X. Hou, J. Qu and Q. Hu, *J. Environ. Chem. Eng.*, 2023, **11**, 110292.
32 L. X. Pan, L. G. Mao, H. N. Zhang, P. P. Wang, C. Wu, J. Xie, B. C. Yu, M. U. Sial, L. Zhang, Y. N. Zhang, L. Z. Zhu, H. Y. Jiang, Y. Q. Zheng and X. G. Liu, *Appl. Sci.*, 2022, **12**(22), 11544.
33 X. Xu, Y. Weng, J. Zhuang, H. Pei, B. Wu, W. Wu, J. Yang, B. Wang and T. Huang, *J. Taiwan Inst. Chem. Eng.*, 2024, **161**, 105541.
34 H. T. Jiang, X. Li and Y. J. Dai, *Environ. Pollut.*, 2024, **341**, 122887.
35 Y. C. Jiang, C. Ming, K. Sun, L. J. Zhang, S. Zhang, Z. H. Cui, D. Wang, C. J. Leng and X. Hu, *Sustainable Mater. Technol.*, 2024, **39**, e00815.
36 Q. Liu, D. Li, H. Cheng, J. Cheng, K. Du, Y. Hu and Y. Chen, *Bioresour. Technol.*, 2021, **329**, 124922.

© 2026 The Author(s). Published by the Royal Society of Chemistry

Open Access Article. Published on 18 May 2026. Downloaded on 5/20/2026 7:35:47 PM. This article is licensed under a Creative Commons Attribution-NonCommercial 3.0 Unported Licence.

37 T. K. T. Nguyen, T. B. Nguyen, W. H. Chen, C. W. Chen, A. K. Patel, X. T. Bui, L. Chen, R. R. Singhania and C. D. Dong, *Bioresour. Technol.*, 2023, **371**, 128593.
38 F. Suo, X. You, Y. Ma and Y. Li, *Chemosphere*, 2019, **235**, 918–925.
39 F. Wei, Y. W. Zhu, T. M. He, S. P. Zhu, T. H. Wang, C. Y. Yao, C. L. Yu, P. P. Huang, Y. Li, Q. Zhao and W. G. Song, *ACS Omega*, 2022, **7**, 46288–46302.
40 B. Zhang, Y. Wu and L. Cha, *J. Dispersion Sci. Technol.*, 2020, **41**, 125–136.
41 D. M. Juela, *Sep. Purif. Technol.*, 2022, **284**, 120286.
42 A. Sridhar, M. Ponnuchamy, A. Kapoor and S. Prabhakar, *J. Hazard. Mater.*, 2022, **424**, 127432.
43 N. Sharma, D. P. Tiwari and S. K. Singh, *Int. J. Res. Ayurveda Pharm.*, 2014, **5**(2), 84–88.
44 H. H. Ngo, W. Guo, T. H. Nguyen, T. M. L. Luong, X. H. Nguyen, T. L. A. Phan and M. K. Nguyen, *Bioresour. Technol.*, 2023, **385**, 129384.
45 M. Thommes, K. Kaneko, A. V. Neimark, J. P. Olivier, F. Rodriguez-Reinoso, J. Rouquerol and K. S. W. Sing, *Pure Appl. Chem.*, 2015, **87**, 1051–1069.
46 R. Gnanasambandam and A. Proctor, *Food Chem.*, 2000, **68**(3), 327–332.
47 N. V. Farinella, G. D. Matos and M. A. Z. Arruda, *Bioresour. Technol.*, 2007, **98**(10), 1940–1946.
48 L. C. Cao, I. K. M. Yu, D. C. W. Tsang, S. C. Zhang, Y. S. Ok, E. E. Kwon, H. Song and C. S. Poon, *Bioresour. Technol.*, 2018, **267**, 242–248.
49 L. Kennedy, J. Vijaya and G. Sekaran, *Ind. Eng. Chem. Res.*, 2004, **43**(8), 1832–1838.
50 M. S. Shafeeyan, W. M. A. W. Daud, A. Houshmand and A. Shamiri, *J. Anal. Appl. Pyrolysis*, 2010, **89**(2), 143–151.
51 J. Georgin, D. S. P. Franco, K. da Boit Martinello, E. C. Lima and L. F. O. Silva, *J. Environ. Chem. Eng.*, 2022, **10**, 107798.
52 G. Yin, X. Chen, B. Sarkar, N. S. Bolan, T. Wei, H. Zhou and H. Wang, *Chem. Eng. J.*, 2023, **466**, 143199.
53 Y. S. Ho, *J. Hazard. Mater.*, 2006, **136**, 681–689.
54 J. Wang and X. Guo, *J. Hazard. Mater.*, 2020, **390**, 122156.
55 J. Wang and X. Guo, *Chemosphere*, 2022, **309**, 136732.
56 A. Srikhaow, W. Chaengsawang, T. Kiatsiriroat, P. Kajitvichyanukul and S. M. Smith, *Minerals*, 2022, **12**, 528.
57 Y. Wang, C. Wang, X. Huang, Q. Zhang, T. Wang and X. Guo, *Chemosphere*, 2024, **349**, 140736.
58 J. Wang and X. Guo, *Chemosphere*, 2020, **258**, 127279.
59 A. Mandal, N. Singh and T. J. Purakayastha, *Sci. Total Environ.*, 2017, **577**, 376–385.
60 P. Zhang, H. Sun, C. Ren, L. Min and H. Zhang, *Environ. Pollut.*, 2018, **234**, 812–820.
61 B. Gámiz, P. Velarde, K. A. Spokas, R. Celis and L. Cox, *Geoderma*, 2019, **337**, 341–349.
62 M. Essandoh, D. Wolgemuth, C. U. Pittman, D. Mohan and T. Mlsna, *Chemosphere*, 2017, **174**, 49–57.
63 L. Min, J. Tang, M. Rafiq and H. Sun, *Biochar*, 2020, **2**, 329–341.
64 J. Jin, M. Kang, K. Sun, Z. Pan, F. Wu and B. Xing, *Sci. Total Environ.*, 2016, **550**, 504–513.
65 L. Wei, L. X. Huang, X. Li, Y. F. Huang, W. S. Chen, R. Ma and Z. Z. Liu, *Agronomy*, 2024, **14**(6), 1290.
66 E. Sormo, L. Silvani, N. Njerkli, N. Hagemann, A. R. Zimmerman, S. E. Hale, C. B. Hansen, T. Hartnik and G. Cornelissen, *Sci. Total Environ.*, 2021, **763**, 144034.
67 E. Sormo, C. B. M. Lade, J. J. Zhang, A. G. Asimakopoulos, G. W. Åsli, M. Hubert, A. I. Goranov, H. P. H. Arp and G. Cornelissen, *Sci. Total Environ.*, 2024, **922**, 170971.
68 Q. Hu and Z. Zhang, *J. Mol. Liq.*, 2019, **277**, 646–648.
69 B. Mahanty, S. K. Behera and N. K. Sahoo, *Sep. Sci. Technol.*, 2023, **58**, 1275–1282.
70 V. Puccia and M. J. Avena, *Colloid Interface Sci. Commun.*, 2021, **41**, 100376.
71 H. N. Tran, E. C. Lima, R. S. Juang, J. C. Bollinger and H. P. Chao, *J. Environ. Chem. Eng.*, 2021, **9**(6), 106674.

© 2026 The Author(s). Published by the Royal Society of Chemistry